Dalton Transactions

PAPER

View Article Online
View Journal | View Issue

Cite this: *Dalton Trans.*, 2016, **45**, 1007

Crystal structure evolution and luminescence properties of color tunable solid solution phosphors $Ca_{2+x}La_{8-x}(SiO_4)_{6-x}(PO_4)_xO_2:Eu^{2+}$

Yufei Xia,[a] Jian Chen,[a] Yan-gai Liu,*[a] Maxim S. Molokeev,[b,c] Ming Guan,[a] Zhaohui Huang[a] and Minghao Fang[a]

Received 28th September 2015,
Accepted 23rd November 2015

DOI: 10.1039/c5dt03786g

www.rsc.org/dalton

A series of apatite solid solution phosphors $Ca_{2+x}La_{8-x}(SiO_4)_{6-x}(PO_4)_xO_2:Eu^{2+}$ (x = 0,2,4,6) were synthesized by a conventional high-temperature solid-state reaction. The phase purity was examined using XRD, XPS and XRF. The crystal structure information, such as the concentration, cell parameters and occupation rate, was analyzed using a Rietveld refinement, demonstrating that the Eu^{2+} activated the $Ca_2La_8(SiO_4)_6O_2$ and $Ca_8La_2(PO_4)_6O_2$ to form continuous solid solution phosphors. Different behaviors of luminescence evolution in response to structural variation were verified among the series of phosphors. Two kinds of Eu^{2+} ion sites were proved using low temperature PL spectra (8k) and room temperature decay curves. The substitution of large La^{3+} ions by small Ca^{2+} ions induced a decreased crystal field splitting of the Eu^{2+} ions, which caused an increase in emission energy from the 5d excited state to the 4f ground state and a resultant blue-shift from 508 nm to 460 nm. Therefore, with the crystal structure evolution, the emitted color of the series of phosphors could be tuned from green to blue by adjusting the ratio of Ca/La.

1. Introduction

Compared to conventional incandescent or fluorescent lamps, LED-based lighting devices fabricated by coating the yellow-emitting phosphor YAG: Ce^{3+} on blue InGaN LED chips have incited a revolution in the lamp industry due to their many advantages, such as significant power reduction, longer lifetime, higher luminous efficiency, environmental friendliness and brightness.[1–3] However, this combination exhibits a poor color rendering index (CRI ≈ 70–80) and a high correlated color temperature (CCT ≈ 7750 K) attributed to the insufficient red emission.[4,5] One solution is to assemble LEDs by pumping a near-ultraviolet (n-UV) emitting chip with a mixture of blue, green and red emitting phosphors, which can then emit high quality white light with a smoother spectral distribution over the whole visible range.[6,7]

The crystal field strength and coordination environment have great influences on the outermost electron transition of the Eu^{2+} ion, the most frequently used activator in phosphors, because the active electronic level is not shielded against the surrounding ligands,[8–10] indicating that Eu^{2+} ions can emit light from the ultraviolet to the infrared with broadband emitting fluorescence.[11,12] It is well known that apatite structure compounds (space group $P6_3/m$), with a general chemical formula of the form $A_{10}(XO_4)_6Z_2$ (A = Ca^{2+},Ba^{2+},Ce^{3+},La^{3+},Y^{3+}, *etc.*, X = P^{5+},As^{5+},Si^{4+}, *etc.*, and Z = O^{2-},F^-,Cl^-,OH^-, *etc.*),[13] contain two kinds of cation sites: the 9-fold coordinated 4f sites with C_3 point symmetry and the 7-fold coordinated 6 h sites with a C_S point symmetry, which are suitable for the substitution of various rare-earth-metal ions.[14–16] Consequently, due to their adjustable structures, and excellent thermal and physicochemical stabilities, apatite compounds have become highly efficient host materials for the luminescence of various rare earth ions and have aroused widespread attention.[17–19] As discussed above, the coordination environment of the Eu^{2+} site is anticipated to be changed *via* chemical composition variation among solid solution phosphors.[20] Thus, the emitted color can be controlled by doping Eu^{2+} ions into a series of apatite solid solution hosts which are expected to display adjustable emission spectra in a wide range to meet the requirements of multi-color phosphors.

In this study, the coordination environment variation of the Eu^{2+} ion has been realized by the replacement of Ca^{2+} ions with La^{3+} ions and resulted in crystal splitting decreases of the Eu^{2+} ion, a series of color tunable solid solution phosphors

[a]*School of Materials Science and Technology, Beijing Key Laboratory of Materials Utilization of Nonmetallic Minerals and Solid Wastes, National Laboratory of Mineral Materials, China University of Geosciences, Beijing, 100083, China. E-mail: liuyang@cugb.edu.cn*
[b]*Laboratory of Crystal Physics, Kirensky Institute of Physics, SB RAS, Krasnoyarsk 660036, Russia*
[c]*Department of Physics, Far Eastern State Transport University, Khabarovsk 680021, Russia*

$Ca_{2+x}La_{8-x}(SiO_4)_{6-x}(PO_4)_xO_2:Eu^{2+}$ (x = 0,2,4,6) were successfully prepared by a high-temperature solid-state reaction. Moreover, it's worth noting that the replacement of $[PO_4]^{3-}$ with the $[SiO4]^{4-}$ tetrahedron was introduced into the solid solution to realize the charge compensation because of the different valences between Ca^{2+}–La^{3+} and also that the $Ca_4La_6(SiO_4)_4(PO_4)_2O_2:Eu^{2+}$ and $Ca_6La_4(SiO_4)_2(PO_4)_4O_2:Eu^{2+}$ phosphors were synthesized for the first time.

The phase purity was demonstrated by XRD, XPS and XRF, and the crystal structure information was analyzed base on Rietveld refinement results. In addition, the relationship between the crystal structure evolutions, the PLE and PL spectra at normal and low temperatures, the lifetimes and the temperature dependence spectra have been discussed in detail.

2. Experimental

2.1. Materials and synthesis

A series of apatite solid solution phosphors $Ca_{2+x}La_{8-x}(SiO_4)_{6-x}(PO_4)_xO_2:0.02Eu^{2+}$ (x = 0,2,4,6) were synthesized according to a conventional high-temperature solid-state method. Ca_2CO_3 (analytical reagent (A. R.)), La_2O_3 (A. R.), SiO_2 (A. R.), $NH_4H_2PO_4$ (A. R.), and Eu_2O_3 (A. R.) were used as the raw materials. After the raw materials were well ground in an agate mortar for 10 min according to the stoichiometric amounts of reactants, all the materials were preheated for 1 h at 1000 °C in a corundum crucible to eliminate H_2O and CO_2. Then, the mixed powders were sintered at 1525 °C in a reductive atmosphere (H_2 10%, N_2 90%) for 6 h in a horizontal tube furnace. Finally, the sintered products were well ground after cooling down to room temperature.

2.2. Characterization

The X-ray diffraction (XRD) data of the powder samples were collected on an X-ray powder diffractometer (D/max-IIIA, Rigaku, Japan) with a step-wise scanning mode over the 2θ range of 10°–110° using Cu Kα radiation (1.5406 Å) under an operating voltage (40 kV) and current (100 mA). The XRD patterns, which were submitted for Rietveld refinement, were acquired at a step size of 0.02° with a counting time of 2 s per step.

X-ray photoelectron spectroscopy (XPS) measurements were collected using a Kratos Axis Ultra DLD, employing an MCP stack & delay-line photoelectron detector with scanned & snapshot spectroscopy modes. X-ray Fluorescence (XRF) measurements were measured by utilizing a Rigaku ZSX Primus II X-ray fluorescence spectrograph. The photoluminescence emission (PL) and the photoluminescence excitation (PLE) spectra at 298k and 8k were measured using a Hitachi F-4600 fluorescence spectrophotometer (Japan) equipped with a 150 W Xe lamp as the excitation source. The temperature-dependent luminescence properties were measured on the same spectrophotometer which was assembled with a computer-controlled electric furnace and a self-made heating attachment. The morphology was observed using high-resolution transmission electron microscopy (HRTEM; JEM-21000, JEOL, Japan). The room-temperature luminescence decay curves were obtained from a spectrofluorometer (Horiba, Jobin Yvon TBXPS) using a tunable pulse laser radiation (nano-LED) for the excitation.

3. Results and discussion

3.1. Phase formation and structural characteristics

The XRD patterns of $Ca_{2+x}La_{8-x}(SiO_4)_{6-x}(PO_4)_xO_2:0.02Eu^{2+}$ (x = 0,2,4,6) and the standard PDF card (JCPDF 29-0337) of $Ca_2La_8(SiO_4)_6O_2$ are displayed in Fig. 1a. All the diffraction peaks of these samples matched well with the JCPDF 29-0337 card, indicating that the series of solid solution phosphors had been prepared successfully and that the introduction of the Eu^{2+} ion did not cause any impurity phase. In addition, the diffraction peaks of the last three samples (x = 2, 4, 6) have obviously shifted towards the high degrees with the increase of the ratio

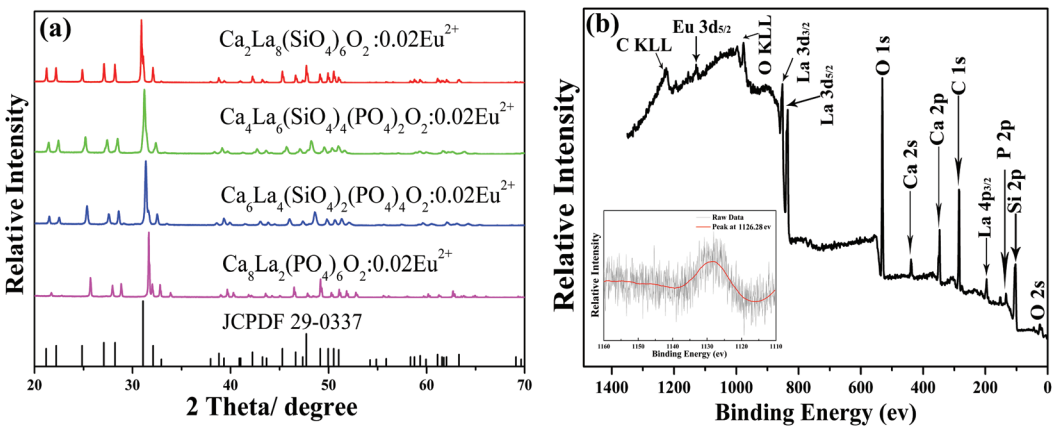

Fig. 1 (a) The XRD patterns of $Ca_{2+x}La_{8-x}(SiO_4)_{6-x}(PO_4)_xO_2:0.02Eu^{2+}$ (x = 0,2,4,6) and the standard PDF card (JCPDF 29-0337) of $Ca_2La_8(SiO_4)_6O_2$. (b) The photoelectron survey spectra of the $Ca_6La_4(SiO_4)_2(PO_4)_4O_2:0.02Eu^{2+}$ sample. The inset shows the high-resolution XPS spectra at the Eu $3d_{5/2}$ position.

of Ca/La. This can be explained as the substitution of the large La^{3+} ion by the small Ca^{2+} ion and the large $[SiO_4]^{4-}$ tetrahedron by the small $[PO_4]^{3-}$ tetrahedron causes a decrease in the lattice constant of the $Ca_{2+x}La_{8-x}(SiO_4)_{6-x}(PO_4)_xO_2$ hosts,[21] which is also evidence demonstrating the existence of a solid solution in the whole range (x = 0,2,4,6).[9] The photoelectron survey spectrum of the $Ca_6La_4(SiO_4)_2(PO_4)_4O_2$:0.02$Eu^{2+}$ sample is plotted in Fig. 1b, depicting photoelectron peaks corresponding to O 2s, Si 2p, P 2p, La $4p_{3/2}$, Ca 2p, Ca 2s, O 1s, La $3d_{5/2}$, La $3d_{3/2}$ and Eu $3d_{5/2}$ emission. The inset shows the high-resolution XPS spectrum at the Eu $3d_{5/2}$ position, and the peak at 1126.28 ev agrees well with the signal of Eu^{2+} $3d_{5/2}$, demonstrating the existence of the Eu^{2+} ion. Furthermore, the elemental content of the $Ca_6La_4(SiO_4)_2(PO_4)_4O_2$:0.02$Eu^{2+}$ sample was further examined and calculated by XRF. As shown in Table 1, the proportions of all components match well with the suggested formula.

Fig. 2a displays the crystal structure of the 2 × 2 × 2 unit cells of $Ca_4La_6(SiO_4)_4(PO_4)_2O_2$, which is chosen as the representative. Obviously, $Ca_4La_6(SiO_4)_4(PO_4)_2O_2$ has a layered structure and contains two kinds of cation sites: the inner-laminar site labeled M(I) with the local symmetry C_3 and the inter-laminar site labeled M(II) with the local symmetry C_S.[22] The two kinds of different coordination environment of the cation sites are displayed in Fig. 2b and c. The M(I) site at the 4f site (C_3) was surrounded by 9 oxygen atoms to form a mono-caped square antiprism, which was connected with tetrahedral PO_4/SiO_4 groups, and the M(II) site at the 6 h site (C_S) formed a pentagonal bipyramid with the surrounding 7 oxygen atoms and these bipyramids were connected with each other through a vertex. Theoretically, both the Ca^{2+} ion and the La^{3+} ion are uniformly distributed in the two kinds of cationic sites,[23] illustrating that the ratio of Ca/La is easily changed by adjusting the proportion of raw materials.

Table 1 The main parameters of the XRF measurements

Component	Result	Unit	Intensity	Spectral lines of the element
O	23.5	Mass%	0.0745	O-KA
Si	3.17	Mass%	3.064	Si-KA
P	8.04	Mass%	20.233	P-KA
Ca	18.7	Mass%	35.581	Ca-KA
La	42.5	Mass%	6.245	La-LA
Eu	1.55	Mass%	0.5759	Eu-LA

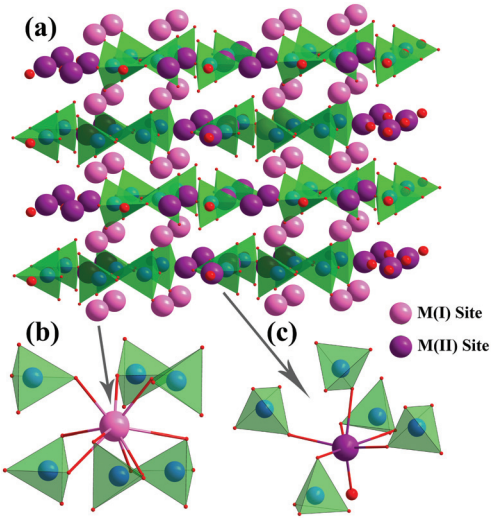

Fig. 2 (a) The crystal structure of the 2 × 2 × 2 unit cells of $Ca_4La_6(SiO_4)_4(PO_4)_2$:0.02$Eu^{2+}$, (b) the coordination environment of the M(I) site with the local symmetry C_3 and (c) the M(II) site with the local symmetry C_S.

The four XRD patterns were analyzed using the Rietveld refinement. The observed (×), calculated (red) and difference (gray) XRD profiles for the refinements of $Ca_{2+x}La_{8-x}(SiO_4)_{6-x}(PO_4)_xO_2$ (x = 0,2,4,6) are shown in Fig. 3a–d. The main refinement parameters of the processing and refinement results are presented in Table 2. The results of the refinement further demonstrate that the series of solid solution phosphors are single phase without any impurity or secondary phases. On the other hand, the ranges of the weighted profile R-factor (R_{wp}) and the R-Bragg factor (R_B) are 10.038%–11.012% and 1.792%–2.777%, respectively, indicating that the crystal structures of these phosphors match well with the starting model ($Ca_2La_8(SiO_4)_6$) after the refinement and that the results are believable and publishable. Meanwhile, we also refined the concentration of these samples while obtaining the high-quality XRD data. According to these refinement results, the calculated formula are $Ca_{2.87(2)}La_{7.13(2)}(SiO_4)_6O_2$, $Ca_{4.47(2)}La_{5.53(2)}(SiO_4)_{3.53(2)}(PO_4)_{2.47(2)}O_2$, $Ca_{5.52(2)}La_{3.48(2)}(SiO_4)_{1.48(2)}(PO_4)_{4.52(2)}O_2$ and $Ca_{8.28(2)}La_{1.72(2)}(PO_4)_6O_2$, demonstrating that the refined concentrations are highly consistent with the suggested formula and that the coordination environment variation is mainly caused by the replacement of a Ca^{2+} with a La^{3+} ion. Moreover, according to the XRD data and the Rietveld refinement, no additive superstructure peaks were detected, this feature proves that the Ca^{2+} ions and the La^{3+} ions were randomly mixed at the atomic level.[24] In addition, the unit lattice parameters and the unit cell volumes of the as-prepared phosphors are given in Fig. 4. The high linear fitting coefficients (0.99334–0.99796) proved the crystal structure evolution of this continuous solid solution. The lattice parameters and unit cell volumes show linear decreases and are proportional to the value of x, which is attributed to the substitution of the large La^{3+} ions by small Ca^{2+} ions, suggesting that the coordination environment of the cations become more unconsolidated as x increases.[25]

As shown in Fig. 5a–d, the linear change in the crystal structure of these solid solution phosphors was further verified by HRTEM and fast Fourier transform (FFT) images. Both the HRTEM and FFT images illustrate that no significant structural defects appeared in the selected areas of these single-phase samples and that good crystallinity was obtained. Moreover, the lattice fringe measurements with the d spacings of 0.315 nm, 0.837 nm, 0.354 nm, and 0.353 nm could be assigned to the planes (210), (010), (021) and (021) for

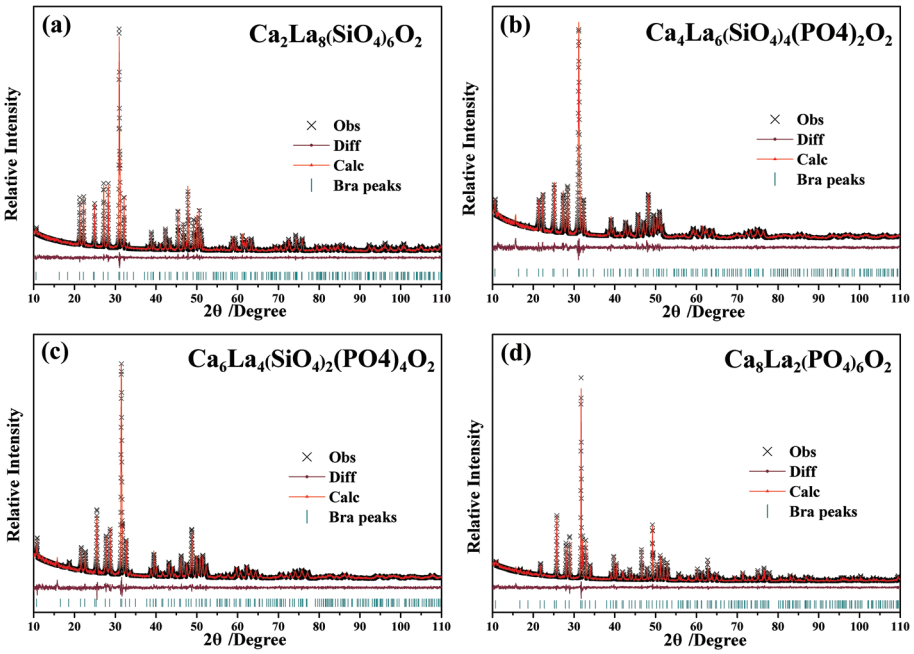

Fig. 3 (a–d) Powder XRD patterns (x) of the $Ca_{2+x}La_{8-x}(SiO_4)_{6-x}(PO_4)_xO_2$:0.02$Eu^{2+}$ (x = 0,2,4,6) samples with the corresponding Rietveld refinement (red) and residuals (gray).

Table 2 The main refinement parameters of $Ca_{2+x}La_{8-x}(SiO_4)_{6-x}(PO_4)_xO_2$ (x = 0,2,4,6)

Compound	x = 0	x = 2	x = 4	x = 6
Sp.Gr.	$P6_3/m$	$P6_3/m$	$P6_3/m$	$P6_3/m$
a, Å	9.6559(1)	9.5948(6)	9.5325(4)	9.4606(2)
b, Å	9.6559(1)	9.5948(6)	9.5325(4)	9.4606(2)
c, Å	7.1529(1)	7.0882(5)	7.0206(4)	6.9356(1)
α, °	90	90	90	90
β, °	90	90	90	90
γ, °	120	120	120	120
V, Å^3	577.56(2)	565.12(8)	552.49(6)	537.59(2)
2θ-Interval,	10–110	10–110	10–110	10–110
R_{wp}, %	10.038	11.012	10.135	10.065
R_{exp}, %	1.311	1.299	1.287	1.325
R_B, %	2.268	2.168	1.792	2.777

$Ca_{2+x}La_{8-x}(SiO_4)_{6-x}(PO_4)_xO_2$:0.02$Eu^{2+}$ (x = 0,2,4,6). The measured d spacing in different orientations could be transformed into the same d spacing value of (021) according to the classic Bragg equation.[24] Therefore, the normalized d spacings of (021) were calculated to be 0.358 nm, 0.356 nm, 0.354 nm and 0.353 nm. Consequently, the decrease of the d spacings is well consistent with the refinement results, indicating the existence of structural evolution in the series of solid solutions.

The effective ionic radii of the Ca^{2+} ions are 1.18 (CN = 9) and 1.06 Å (CN = 7) and the effective ionic radii of the La^{3+} ions are 1.21 (CN = 9) and 1.10 Å (CN = 7). Theoretically, considering the similar ionic radius and valence, the Eu^{2+} ion ($R_{CN=9}$ = 1.3, $R_{CN=7}$ = 1.2) is expected to substitute the La^{3+} and Ca^{2+} sites in the $Ca_{2+x}La_{8-x}(SiO_4)_{6-x}(PO_4)_xO_2$ (x = 0,2,4,6) crystal structure.[26] Therefore, four kinds of emitting blocks will be included in the host: Ca(I), Ca(II), La(I) and La(II). The occupation rates of Ca(I), Ca(II), La(I), and La(II), reflecting the distribution of Ca^{2+} ions and La^{3+} ions in the two cationic sites, have been refined and displayed in Table 3. When the content of Ca^{2+} ions increases, the occupation rate of La(II) is decreased faster than that of La(I) and the M(II) site is totally occupied by Ca^{2+} ions while the chemical formula is $Ca_8La_2(PO_4)_6O_2$ (x = 6), which shows similar results to the previous studies.[16,26] The phenomenon can be explained as follows: the Eu^{2+} ion located at the M(II) site that is connected with a free oxygen ion, results in a very short Eu–O distance due to the small sum of the electrostatic bond strength of the cations toward the free oxygen ion. Thus, it must be very unfavorable for the (6 h) sites to be occupied by a cation with a large radius in these compounds.[27]

3.2. Photoluminescence characteristics

The PLE spectra (monitored in the range of 460 nm–508 nm) and the PL spectra (under 365 nm excitation) of the $Ca_{2+x}La_{8-x}(SiO_4)_{6-x}(PO_4)_xO_2$:0.02$Eu^{2+}$ (x = 0,2,4,6) phosphors at room temperature are displayed in Fig. 6a and b, respectively. The PLE spectra depict a series of broad excitation bands between 250 nm and 450 nm, which are attributed to the $4f^7 \rightarrow 4f^65d^1$ transition of the Eu^{2+} ion,[28] and the emission spectra show a series of broad emission bands from 400 nm to 650 nm, which are attributed to the 5d → 4f transition of the Eu^{2+} ion. As shown in Fig. 6b, a strong asymmetric broad band with a maximum wavelength peak at 508 nm was detected in the PL spectrum of $Ca_2La_8(SiO_4)_6O_2$:0.02Eu^{2+}, which was

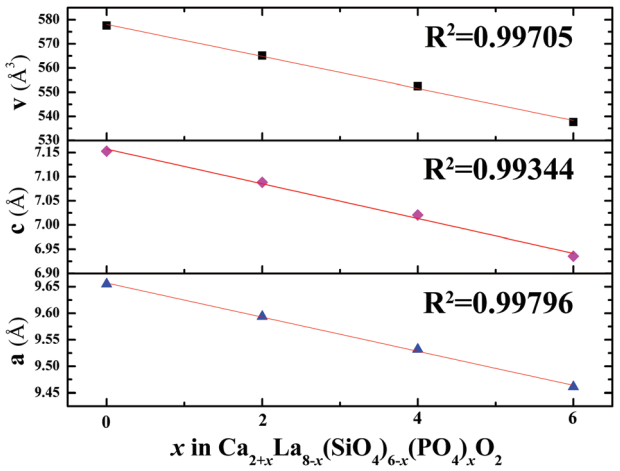

Fig. 4 The refined unit cell parameters (a, c) and cell volume (v) of $Ca_{2+x}La_{8-x}(SiO_4)_{6-x}(PO_4)_xO_2$:0.02$Eu^{2+}$ (x = 0,2,4,6).

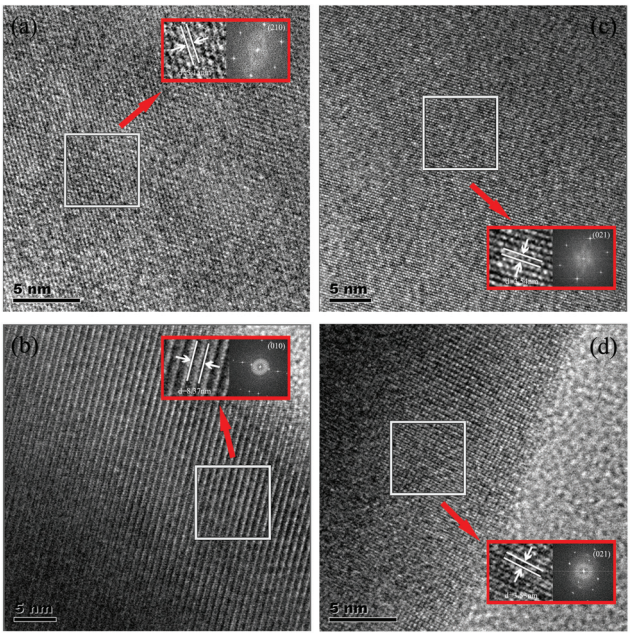

Fig. 5 HRTEM and FFT images for $Ca_{2+x}La_{8-x}(SiO_4)_{6-x}(PO_4)_xO_2$:0.02$Eu^{2+}$ with different x values, x = 0 (a), x = 2 (b), x = 4 (c) and x = 6 (d).

Table 3 Atomic occupation rates in $Ca_{2+x}La_{8-x}(SiO_4)_{6-x}(PO_4)_xO_2$ with different x values

Sites	x = 0	x = 2	x = 4	x = 6
Ca1	0.12(2)	0.20(2)	0.43(1)	0.714(7)
La1	0.88(2)	0.80(2)	0.57(1)	0.286(7)
Ca2	0.53(1)	0.81(1)	0.983(7)	1.000(6)
La2	0.47(1)	0.19(1)	0.017(7)	0.000(6)

chosen as the representative of the solid solution phosphors. The asymmetric emission band can be decomposed into two Gaussian component peaks at 504 nm (I1) and 542 nm (I2) demonstrating the existence of two types of emitting centers in $Ca_2La_8(SiO_4)_6O_2$:0.02Eu^{2+}.

Fig. 6c and d display the low temperature (8k) PLE and PL spectra of $Ca_2La_8(SiO_4)_6O_2$:0.02Eu^{2+} and $Ca_8La_2(PO_4)_6O_2$:0.02Eu^{2+}. The PL spectra of $Ca_2La_8(SiO_4)_6O_2$:0.02Eu^{2+} can be separated into two components with peaks at 526 nm and 576 nm, and the PL spectra of $Ca_8La_2(PO_4)_6O_2$:0.02Eu^{2+} obviously contains two components with peaks at 460 nm and 625 nm. The results further demonstrate that there are two kinds of cation sites included in the series of apatite phosphors which could be occupied by the Eu^{2+} ion.

Actually, considering the valence state and the previous results,[16,29] the blue emission band observed in the PL spectrum of $Ca_2La_8(PO_4)_6O_2$:0.02Eu^{2+} is attributed to the substitution of a Ca^{2+} ion by a Eu^{2+} ion. According to the report by Van Uitert, to further demonstrate the relationship between emission peaks and emission centers, the possible crystallographic site may be investigated theoretically by the following equation:[30]

$$E(\mathrm{cm}^{-1}) = Q^{*}\left[1 - \left(\frac{V}{4}\right)^{1/V} \times 10^{-(nE_a r)/80}\right], \quad (1)$$

where E represents the energy position of the d-band edge for the rare-earth ion (cm^{-1}), Q^{*} is the energy position for the lower d-band edge for the free ion (34 000 cm^{-1} for Eu^{2+}), V is the valence of the activator (Eu^{2+}) ion (V = 2), n is the number of anions in the immediate shell around the Eu^{2+} ion, r is the radius of the host cation replaced by the Eu^{2+} ion (in Å), and E_a is the electron affinity of the atoms that form anions (in eV) depending on the anion complex type. Here, E_a was approximately determined as 1.60 for the $[SiO_4]^{4-}$ in the oxide host[31] and the r values of Ca(I) and Ca(II) were calculated to be 118 pm and 106 pm, respectively. Consequently, the E_{calcd} values of Ca(I) and Ca(II) were calculated to be 19 693 cm^{-1} and 18 546 cm^{-1}, respectively. The results indicated that the emission band centered at 504 nm was attributed to a Eu^{2+} ion occupying the Ca(I) site with C_3 symmetry and nine-coordination and that the emission band peaked at 542 nm was attributed to a Eu^{2+} ion occupying the Ca(II) site with C_S symmetry and seven-coordination.

The emission wavelengths of the $Ca_{2+x}La_{8-x}(SiO_4)_{6-x}(PO_4)_xO_2$:0.02$Eu^{2+}$ (x = 0,2,4,6) PL spectra show a wide blue shift from 508 nm to 460 nm with the increase of the x value which is dependent on the crystal field strength variation. The structural model of the cation substitution around the Eu^{2+} ion sites is depicted in Fig. 7. In this regard, the crystal field splitting of the Eu^{2+} ions can be determined as obeying:[17,32,33]

$$D_q = \frac{ze^2r^4}{6R^5} \quad (2)$$

where D_q is a measure of energy level separation, R represents the distance from the central ion to its ligands, z stands for the charge or valence of the anion, r is the radius of the d wave

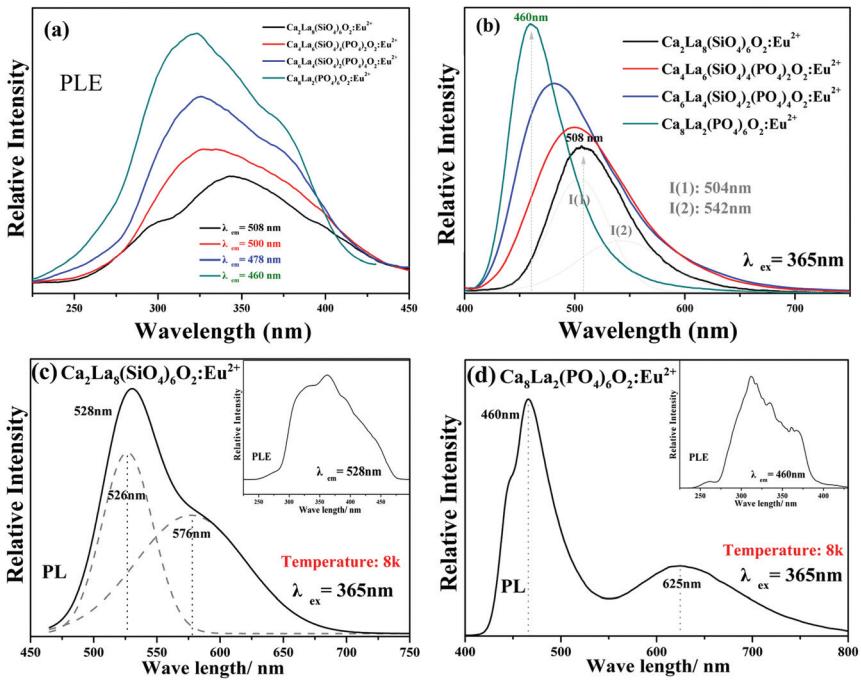

Fig. 6 (a) The PLE monitored in the range of 460 nm–508 nm and (b) the PL spectra under 365 nm excitation of $Ca_{2+x}La_{8-x}(SiO_4)_{6-x}(PO_4)_xO_2$:0.02$Eu^{2+}$ (x = 0,2,4,6) at room temperature. (c) The PL and PLE spectra at low temperature (8k) of $Ca_2La_8(SiO_4)_6O_2$:0.02Eu^{2+} and (d) the PL and PLE spectra at low temperature (8k) of $Ca_8La_2(PO_4)_6O_2$:0.02Eu^{2+}.

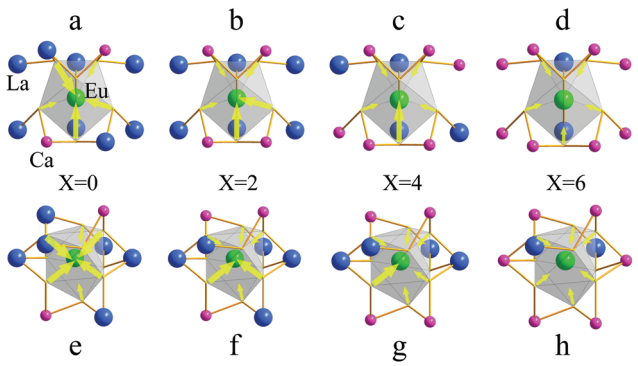

Fig. 7 Structural model for explaining the photoluminescence evolution observed in the $Ca_{2+x}La_{8-x}(SiO_4)_{6-x}(PO_4)_xO_2$:0.02$Eu^{2+}$ (x = 0,2,4,6) phosphors: (a–d) represent Eu^{2+} located in the M(I) site, (e–h) represent Eu^{2+} located in the M(II) site.

function, and e is the charge of an electron. For the $d_{(Eu-O)}$ orbital, if z, e and r are equal, then D_q is only a function of $1/R^5$. When the large La^{3+} ion is substituted by the small Ca^{2+} ion, the distance between Eu^{2+} and O^{2+} becomes longer and the magnitude of the crystal field strength decreases.[34,35] Thus, the crystal field splitting of the Eu^{2+} ion is reasonably decreased and this results in a gradual increase of the lowest 5d state.[36] As a consequence, the emission wavelength shows a blue shift among the as-prepared phosphors and a color variation from green to blue.

In addition, as shown in Table 4, the stokes shifts were estimated to be 6135 cm^{-1}–5985 cm^{-1} and the full width at half-maximum (FWHMs) of the PLE spectra decrease from 142 nm to 113 nm with the increase in x. The crystal-field splitting of the Eu^{2+} ions was estimated to be 22 230 cm^{-1}–18 190 cm^{-1}, which is calculated by the gap between the first and the last component peaks of the PLE spectra. All the computations further demonstrate the decrease of the crystal field splitting.[37]

Furthermore, Fig. 8 presents the room temperature decay curves of the Eu^{2+} ion luminescence in the $Ca_{2+x}La_{8-x}(SiO_4)_{6-x}(PO_4)_xO_2$:0.02$Eu^{2+}$ (x = 0,2,4,6) series. All of the decay curves can be well fitted with a second order exponential equation:

$$I(t) = A_1 \exp(-t/\tau_1) + A_2 \exp(-t/\tau_2) \quad (3)$$

where $I(t)$ is the luminescence intensity, A_1 and A_2 represent constants, τ is the time, and τ_1 and τ_2 stand for rapid and

Table 4 Excitation and emission bands, stokes shift, and the crystal field splitting of the $Ca_{2+x}La_{8-x}(SiO_4)_{6-x}(PO_4)_xO_2$:0.02$Eu^{2+}$ (x = 0,2,4,6) phosphors

x Values	λ_{ex} range (nm)	FWHM of λ_{ex} (nm)	λ_{em} (nm)	Stokes shift (cm^{-1})	Crystal field splitting (cm^{-1})
0	250–450	142	508	6135	22 230
2	250–450	127	500	6082	20 833
4	250–450	118	478	6039	19 231
6	250–400	113	460	5985	18 190

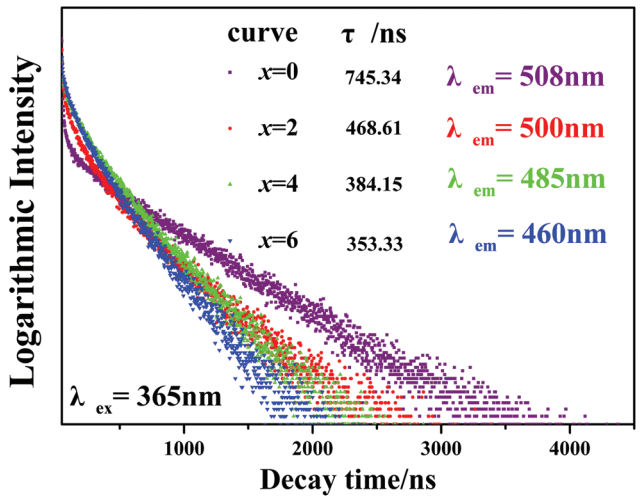

Fig. 8 Room temperature decay curves of the $Ca_{2+x}La_{8-x}(SiO_4)_{6-x}(PO_4)_xO_2:0.02Eu^{2+}$ (x = 0,2,4,6) phosphors.

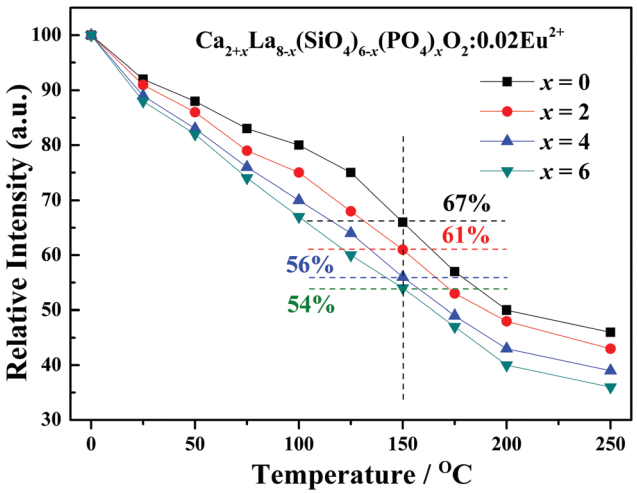

Fig. 9 The peak emission intensity of temperature dependence that normalized to 25 °C values.

slow lifetimes for exponential components, respectively. Moreover, the effective lifetime constant (τ*) can be calculated as:

$$\tau* = (A_1\tau_1{}^2 + A_2\tau_2{}^2)/(A_1\tau_1 + A_2\tau_2) \quad (4)$$

The effective decay times were calculated to be 745.34, 468.61, 384.15 and 353.33 ns with x = 0, 2, 4 and 6, respectively. One can see that the decay times decrease with the increasing Ca^{2+} ion content. Due to the phase structures becoming more unconsolidated compared to the original $Ca_2La_8(SiO_4)_4:0.02Eu^{2+}$ phase, the increasing possibility of energy transfer among the Eu^{2+} ions increases the possible non-radiative transition and leads to the decreasing lifetime values.[32,38] Also the two decay components (τ_1 and τ_2) proved that the Eu^{2+} occupied two different Ca^{2+} sites.[13]

The temperature dependence experiment proved that the thermal stability is consistent with the crystal structure evolution in the as-prepared series phosphors, and the peak emission intensity that normalized to 25 °C values was depicted in Fig. 9. As shown in Fig. 9, the emission intensity of all the samples decreases with the increase in temperature. Additionally, the thermal stability gradually decreases with the increasing x values, this phenomenon can be explained by the neighboring-cation effect.[39,40] The replacement of large La^{3+} ions by small Ca^{2+} ions makes the distances between the Eu^{2+} activator ion and the neighboring cations become smaller, as demonstrated by the refined cell parameters and cell volume, resulting in a larger coulombic force following the inverse-square law[41,42] and the decrease of the thermal quenching barrier height. Thus, the thermal stability becomes lower when the replacement occurs.

Luminescence efficiency is an important technological parameter for the application of phosphors. The internal quantum efficiency (QE) of the $Ca_{2+x}La_{8-x}(SiO_4)_{6-x}(PO_4)_xO_2:0.02Eu^{2+}$ (x = 0,2,4,6) phosphors was measured and calculated following:[12]

$$\eta_{QE} = \frac{\int L_S}{\int E_R + \int E_S} \quad (5)$$

where L_S is the luminescence emission spectrum of the sample, E_R represents the spectrum of the excitation light from the empty integrated sphere (without the sample), and E_S stands for the excitation spectrum for exciting the sample. As a result, under 365 nm excitation, the internal QE of the $Ca_{2+x}La_{8-x}(SiO_4)_{6-x}(PO_4)_xO_2:0.02Eu^{2+}$ (x = 0,2,4,6) phosphors was estimated to be about 45.44%, 46.39%, 44.12% and

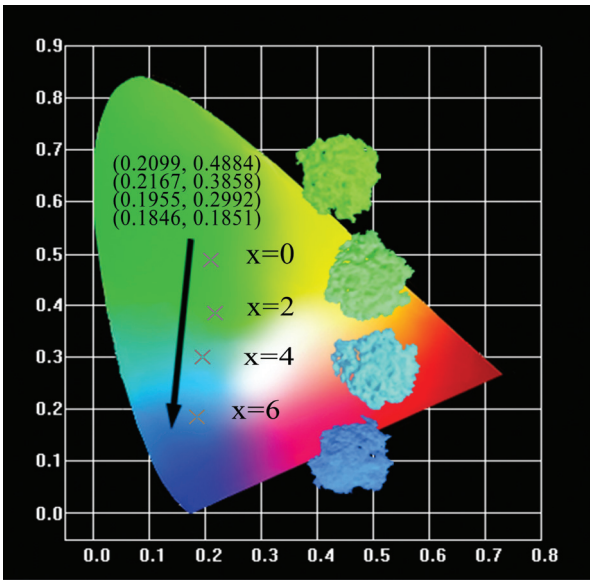

Fig. 10 The CIE coordinates and the digital photos of the $Ca_{2+x}La_{8-x}(SiO_4)_{6-x}(PO_4)_xO_2:0.02Eu^{2+}$ (x = 0,2,4,6) phosphors.

46.56% for x = 0, 2, 4, and 6, respectively. The QE of the as-prepared phosphors can be further optimized by improving the preparation conditions because the QE depends closely on the prepared conditions, crystalline defects, particle sizes and the morphology of the phosphor.[25,39]

The CIE coordinates and the digital photos of the $Ca_{2+x}La_{8-x}(SiO_4)_{6-x}(PO_4)_xO_2$:0.02$Eu^{2+}$ (x = 0,2,4,6) phosphors under 365 nm excitation are displayed in Fig. 10. The calculated CIE coordinates are (0.2099, 0.4884) for x = 0, (0.2167, 0.3585) for x = 2, (0.1955, 0.2992) for x = 4 and (0.1846, 0.1851) for x = 6. Obviously, both the digital photos and the coordinates demonstrate that the emitted color of the solid solution phosphors $Ca_{2+x}La_{8-x}(SiO_4)_{6-x}(PO_4)_xO_2$:0.02$Eu^{2+}$ (x = 0,2,4,6) can be adjusted in the wide range from green to blue by changing the ratio of Ca/La.

4. Conclusions

In summary, a series of continuous solid solution phosphors $Ca_{2+x}La_{8-x}(SiO_4)_{6-x}(PO_4)_xO_2$:0.02$Eu^{2+}$ (x = 0,2,4,6) were successfully synthesized by a solid-state reaction method. The phase purity was examined by XRD, XPS and XRF, the crystal structure information was identified by both Rietveld refinement and HRTEM. The refined concentration, cell parameters and occupation rate matched well with the suggested formula and the variation tendency of Ca/La demonstrating that Eu^{2+} activated $Ca_2La_8(SiO_4)_6O_2$ and $Ca_8La_2(PO_4)_6O_2$ to form continuous solid solution phosphors. Different spectroscopic behavior properties based on structural variations were verified among the series of phosphors. The PL spectra at room temperature and low temperature (8k) were well separated into two component peaks, demonstrating that there are two kinds of Eu^{2+} ion sites included in these apatite phosphors. Furthermore, the short wavelength emission peak is from the Eu^{2+} ion located at the 4f site with nine coordination and the long wavelength emission peak is ascribed to the Eu^{2+} ion occupying the 6 h site with seven coordination. Under 365 nm excitation, the series of phosphors show a strong blue shift from 508 nm to 460 nm. It can be explained by the fact that the substitution of the large La^{3+} ions by small Ca^{2+} ions induced a decreased crystal field splitting of the Eu^{2+} ions, which led to the emission energy from the 5d excited state to the 4f ground state increasing. Consequently, the emitted color of the series of phosphors could be tuned from green to blue by adjusting the ratio of Ca/La.

Acknowledgements

This work was sponsored by National Natural Science Foundation of China (Grant No. 51472223), the Program for New Century Excellent Talents in University of Ministry of Education of China (Grant No. NCET-12-0951) and the Fundamental Research Funds for the Central Universities (Grant No. 2652015020).

References

1 W. R. Liu, C. H. Huang, C. W. Yeh, J. C. Tsai, Y. C. Chiu, Y. T. Yeh and R. S. Liu, *Inorg. Chem.*, 2012, **51**, 9636.
2 H. Wu, X. M. Zhang, C. F. Guo, J. Xu, M. M. Wu and Q. Su, *IEEE Photonics Technol. Lett.*, 2015, **17**, 1160–1162.
3 X. J. Zhang, L. Huang, F. J. Pan, M. M. Wu, J. Wang, Y. Chen and Q. Su, *ACS Appl. Mater. Interfaces*, 2014, **6**, 2709–2717.
4 M. M. Shang, D. L. Geng, D. M. Yang, X. Kang, Y. Zhang and J. Lin, *Inorg. Chem.*, 2013, **52**, 3102–3112.
5 Z. G. Xia, Y. Y. Zhang, M. S. Molokeev and V. V. Atuchin, *J. Phys. Chem. C*, 2013, **117**, 20847–20854.
6 J. Chen, Y. G. Liu, M. H. Fang and Z. H. Huang, *Inorg. Chem.*, 2014, **53**, 11396–11407.
7 X. J. Zhang, J. Wang, L. Huang, F. J. Pan, Y. Chen, B. F. Lei, M. Y. Peng and M. M. Wu, *ACS Appl. Mater. Interfaces*, 2015, **7**, 10044–10054.
8 J. Chen, Y. G. Liu, H. K. Liu, H. Ding, M. H. Fang and Z. H. Huang, *Opt. Mater.*, 2015, **42**, 80–86.
9 M. Zhang, J. Wang, Z. Zhang, Q. Zhang and Q. Su, *Appl. Phys. B: Lasers Opt.*, 2008, **93**, 829–835.
10 K. H. Kwon, W. B. Im, H. S. Jang, H. S. Yoo and D. Y. Jeon, *Inorg. Chem.*, 2009, **48**, 11525–11532.
11 P. Dorenbos, *J. Lumin.*, 2003, **104**, 239–260.
12 J. Chen, Y. G. Liu, L. F. Mei, H. K. Liu, M. H. Fang and Z. H. Huang, *Sci. Rep.*, 2015, **14**, 13258.
13 Z. Xia, M. S. Molokeev, W. B. Im, S. Unithrattil and Q. Liu, *J. Phys. Chem. C*, 2015, **119**, 9488–9495.
14 G. Zhu, Y. R. Shi, M. Mikami, Y. Shimomura and Y. H. Wang, *Opt. Mater.*, 2013, **3**, 229–236.
15 H. K. Liu, Y. Y. Zhang, L. B. Liao, Q. F. Guo and L. F. Mei, *Ceram. Int.*, 2014, **40**, 13709–13713.
16 M. M. Shang, G. G. Li, D. L. Geng, D. M. Yang, X. J. Kang, Y. Zhang, H. Z. Lian and J. Lin, *J. Phys. Chem. C*, 2012, **116**, 10222–10231.
17 N. Guo, H. P. You, C. Z. Ji, R. Z. Ouyang and D. H. Wu, *Dalton Trans.*, 2014, **43**, 12373–12379.
18 G. G. Li, Y. Zhang, D. L. Geng, M. M. Shang, C. Peng and J. Lin, *ACS Appl. Mater. Interfaces*, 2012, **4**, 296–305.
19 Y. Zhang, G. G. Li, D. L. Geng, M. M. Shang, C. Peng and J. Lin, *Inorg. Chem.*, 2012, **51**, 11655–11664.
20 H. P. Ji, Z. H. Huang, Z. G. Xia, M. S. Molokeev, V. V. Atuchin, M. H. Fang and Y. G. Liu, *J. Phys. Chem. C*, 2015, **119**, 2038–2045.
21 Y. R. Do, K. Y. Ko, S. H. Na and Y. D. Huh, *J. Electrochem. Soc.*, 2006, **153**, 142–146.
22 F. M. Ryan, R. W. Warren, R. H. Hopkins and J. Murphy, *J. Electrochem. Soc.*, 1978, **125**, 1493–1498.
23 W. Y. Huang, F. Yoshimure, K. Ueda, Y. Shimomura, H. S. Sheu, T. S. Chen, H. F. Greer, W. Z. Zhou, S. F. Hu, R. S. Liu and J. P. Attfield, *J. Am. Chem. Soc.*, 2012, **134**, 14108.
24 Z. Xia, Y. Zhang, M. S. Molokeev, V. V. Atuchin and Y. Luo, *Sci. Rep.*, 2013, **3**, 3310.

25 K.-W. Huang, W.-T. Chen, C.-I. Chu, S.-F. Hu, H.-S. Sheu, B.-M. Cheng, J.-M. Chen and R.-S. Liu, *Chem. Mater.*, 2012, **24**, 2220–2227.
26 R. E. Ouenzerfia, G. Panczera, C. Goutaudiera, M. T. Cohen-Adada, G. Boulona, M. Trabelsi-Ayedib and N. Kbir-Ariguibc, *Opt. Mater.*, 2001, **16**, 301–310.
27 G. Li, D. Geng, M. Shang, Y. Zhang, C. Peng, Z. Cheng and J. Lin, *J. Phys. Chem. C*, 2011, **115**, 21882–21892.
28 G. Blasse, W. L. Wanmaker, J. W. Tervrugt and A. Bril, *Philips Res. Rep.*, 1968, **23**, 189–200.
29 B. Lee, S. Lee, H. G. Jeong and K. S. Sohn, *ACS Comb. Sci.*, 2011, **13**, 154–158.
30 V. Uitert, *J. Lumin.*, 1984, **29**, 1–9.
31 H. P. Ji, Z. H. Huang, Z. G. Xia, M. S. Molokeev, X. X. Jiang, Z. H. Lin and V. V. Atuchin, *Dalton Trans.*, 2015, **44**, 7679–7686.
32 C. Zhao, Z. Xia and S. Yu, *J. Mater. Chem. C*, 2014, **2**, 6032.
33 C.-H. Huang, P.-J. Wu, J.-F. Lee and T.-M. Chen, *J. Mater. Chem.*, 2011, **21**, 10489.
34 P. Dorenbos, *Phys. Rev. B: Condens. Matter*, 2001, **64**, 117–125.
35 K. A. Denault, J. Brgoch, M. W. Gaultois, A. Mikhailovsky, R. Petry, H. Winkler, S. P. DenBaars and R. Seshadri, *Chem. Mater.*, 2014, **26**, 2275–2282.
36 C. H. Huang, Y. C. Chiu, Y. T. Ye, T. S. Chan and T. M. Chen, *ACS Appl. Mater. Interfaces*, 2012, **4**, 6661–6668.
37 G. P. Dong, X. D. Xiao, L. L. Zhang, Z. J. Ma, X. Bao, M. Y. Peng, Q. Y. Zhang and J. R. Qiu, *J. Mater. Chem.*, 2011, **21**, 2194–2203.
38 J. Zhou, Z. Xia, M. Chen, M. S. Molokeev and Q. Liu, *Sci. Rep.*, 2015, **5**, 12149.
39 N. Guo, Y. Zheng, Y. Jia, H. Qiao and H. You, *J. Phys. Chem. C*, 2012, **116**, 1329–1334.
40 W. Y. Huang, F. Yoshimure, K. Ueda, Y. Shimomura, H. S. Sheu, T. S. Chen, H. F. Greer, W. Z. Zhou, S. F. Hu, R. S. Liu and J. P. Attfield, *J. Am. Chem. Soc.*, 2012, **134**, 14108.
41 D. J. Griffiths, *Introduction to Electrodynamics*, Prentice Hall, 3rd edn, 1998, ISBN 0-13-805326-X.
42 Z. Y. Wang, Z. G. Xia, M. S. Molokeev, V. V. Atuchin and Q. L. Liu, *Dalton Trans.*, 2014, **43**, 16800.